Published in final edited form as:
J Vasc Interv Radiol. 2014 March ; 25(3): 397–404. doi:10.1016/j.jvir.2013.10.022.

Localized Hyperthermia with Iron Oxide-Doped Yttrium Microparticles: Steps Towards Image-Guided Thermoradiotherapy in Liver Cancer

Andrew C. Gordon[1,2], **Robert J. Lewandowski**[1], **Riad Salem**[1,3,4], **Delbert E. Day**[5], **Reed A. Omary**[6], and **Andrew C. Larson**[1,2]

[1]Department of Radiology, Northwestern University Feinberg School of Medicine, Chicago, IL, USA

[2]Department of Biomedical Engineering, Northwestern University, Evanston, IL, USA

[3]Department of Medicine-Hematology/Oncology, Northwestern University Feinberg School of Medicine, Chicago, IL, USA

[4]Department of Surgery-Organ Transplantation, Northwestern University Feinberg School of Medicine, Chicago, IL, USA

[5]Department of Materials Science & Engineering, Missouri University of Science and Technology, Rolla, MO, USA

[6]Department of Radiology & Radiological Sciences, Vanderbilt University, Nashville, TN, USA

Abstract

PURPOSE—To test whether iron oxide–containing yttrium aluminosilicate microparticles (IO-YAS MPs) can generate localized therapeutic hyperthermia (≥43°C) when injected intra-tumorally in an animal model of liver cancer and whether MP distributions could be visualized with MR imaging.

MATERIALS AND METHODS—Twenty-one Sprague-Dawley rats implanted with N1-S1 liver tumors were assigned to alternating magnetic field (AMF) exposure following intra-tumoral injection with IO-YAS MPs (*n*=7), sham surgery (*n*=7), or baseline iron quantitation (*n*=7). Three fiber optic probes allowed spatial and temporal monitoring of temperatures during 24 minutes of AMF. T2-weighted turbo spin echo magnetic resonance imaging was performed within 1 hour post-procedure to detect signal voids due to IO-YAS deposition. Hematoxylin and eosin–stained

Corresponding author: Andrew C. Larson, PhD, Department of Radiology, Northwestern University Feinberg School of Medicine, 737 N. Michigan Ave, 16th Floor, Chicago, IL 60611, Tel./fax: (312) 926-3499 / (312) 926-5991, a-larson@northwestern.edu.

This work was presented in part at the 2011 SIR Annual Scientific Meeting in Chicago, Illinois. It was selected for the Dr. Constantin Cope Award and was one of fifteen featured abstracts.

Disclosures: Mr. Gordon: None; Dr. Lewandowski: None; Dr. Salem: Paid consultant for Nordion; Dr. Day: Former owner of Mo-Sci Corporation; Dr. Omary: Co-founder of Interventional Oncology Research and Development, LLC (IORAD); Dr. Larson: Co-founder of Interventional Oncology Research and Development, LCC (IORAD). This study was funded by the National Institutes of Health (NCI R01CA159178, R01CA141047), the SIR Foundation through provision of a Student Research Grant (ACG), and the Department of Radiology of the Feinberg School of Medicine. Histopathology was provided by the Northwestern University Mouse Histology and Phenotyping Laboratory and a Cancer Center Support Grant (NCI CA060553).

pathologic slides were also obtained and the presence of IO-YAS was evaluated with inductively coupled plasma optical emission spectroscopy.

RESULTS—Following AMF exposure, intra-tumoral temperatures after IO-YAS MP injection achieved therapeutic hyperthermia while those after sham surgery did not (46.6±1.3 vs. 36.8±0.4°C, $P<0.0001$). Within the treated group, the normal hepatic parenchyma (NHP) and rectal temperatures were 37.4±0.9 and 36.5±1.0°C ($P=0.0809$) at the conclusion of AMF exposure, respectively. A T2-weighted signal void at the tumor site was observed in 7/7 treated animals and intra-tumoral IO-YAS visualized on subsequent histopathology in each case. The mean ratio of tumor:NHP Fe concentrations attributable to IO-YAS MPs was 108:1.

CONCLUSIONS—AMF exposure of intra-tumoral IO-YAS MPs generates localized therapeutic hyperthermia in an animal model of liver cancer. MR detectability and potential for combination brachytherapy warrants further investigation for thermoradiotherapy in liver cancer.

Introduction

HYPERTHERMIA can serve to synergistically augment radiosensitivity and even improve survival in the treatment of some cancers (1,2). Inhibition of cellular repair mechanisms, enhanced tissue oxygenation, delivery of reactive oxygen species, thermal sensitivity of S-phase cells, and increased lysosomal activity are among the posited sensitization mechanisms (3,4). The combination of hyperthermia and radiation therapy (thermoradiotherapy) has demonstrated significantly improved loco-regional control over radiation therapy alone for accessible tumors of the chest wall, cervix, rectum, bladder, melanoma, head, and neck despite the great variability in delivery and dosing strategies (5). Therefore, hyperthermia may enhance the efficacy of radioembolization procedures for both primary liver tumors and metastases.

In 1957, Gilchrist et al. reported the use of 0.02–0.1μm Fe_2O_3 particles for selective inductive heating of lymph nodes in dogs (6). Contemporary thermoradiotherapy combining magnetic hyperthermia of ferrofluids and external beam radiotherapy was approved for clinical treatment of glioblastoma patients in the European Union (7) and is also being investigated for the treatment of prostate cancer with promising initial results (8). This progress provides important evidence of clinical applicability that may facilitate targeted thermoradiotherapy in liver cancer through similar instrumentation.

The introduction of iron oxide (IO) as an integral component of embolic materials is appealing because it allows for a) rapid and sustained localized heating of targeted tissues with noninvasive, external application of alternating magnetic fields (AMFs) (9), b) MR imaging of embolic material delivery (10), and finally also c) enhanced retention of these materials within tumor tissues and/or vascular beds upon external application of a static magnetic field (11,12). Yttrium aluminosilicate (YAS) microspheres with iron oxide (Fe_2O_3) nanocrystals dispersed throughout the glass matrix permit intra-procedural magnetic resonance imaging (MRI) of intra-hepatic biodistributions following transcatheter delivery (13).

The purpose of this study was to test the hypothesis that magnetically functionalized YAS glass doped with magnetite (Fe_3O_4) nanocrystals can generate AMF hyperthermia for applications in image-guided loco-regional thermoradiotherapy (radioembolization augmented with focal hyperthermia) and allow visualization with MRI. We evaluated the AMF heating properties of non-activated (^{89}Y) IO-YAS microparticles (IO-YAS MPs) in phantoms and demonstrated localized therapeutic hyperthermia (≥43°C) and visualization with MRI when injected within deep-seated liver tumors in an animal model of liver cancer. A control group for the applied AMF was implemented to account for eddy currents or

altered thermoregulatory mechanisms arising from deposited radiofrequency (RF) energy (14).

MATERIALS AND METHODS

Study Design

Our institution's animal care and use committee approved this study in 21 adult Sprague-Dawley male rats (Charles River Laboratories, Wilmington, MA) weighing 301–325g. All rats underwent N1-S1 rat hepatoma cell implantation; each animal was assigned to one of three groups: IO-doped YAS MP injection and AMF exposure, AMF exposure (no particle injection), and control group (no injection, AMF, or MR imaging; only used for baseline ICP-OES, *see below*). Liver and tumor specimens were harvested for both histopathological analysis and inductively coupled plasma optical emission spectroscopy (ICP-OES) measurements for MP detection.

Tumor Implantation

Anesthesia was induced with ketamine (75–100mg/kg) and xylazine (2–6mg/kg) administered by intramuscular injection. N1-S1 cells (ATCC, CRL-1604, Manassas, VA) were maintained in a humidified 5% CO_2 atmosphere at 37°C in Dulbecco's Modified Eagle Medium (Invitrogen, Carlsband, CA) supplemented with 10% fetal bovine serum (Atlanta Biologicals, Lawrenceville, GA), 100U/ml penicillin and 100μg/ml streptomycin (Invitrogen, Carlsband CA). Cells were subcultured every 2–3 days. Cell viability was tested with trypan blue (Mediatech, Inc) staining confirming >90% cell viability before implantation. The left lateral lobe of the liver was exposed following a midline subxiphoid incision and mini-laporotomy. N1-S1 rat hepatoma cells (6×10^6 cells in 0.2ml DMEM) were slowly injected (≥30 seconds) directly under the hepatic capsule. Absorbable hemostatic gauze (LifeScience PLUS, Mountain View CA) was applied at the injection site to prevent reflux and the abdomen was surgically closed in two layers. Tumor growth was allowed for 7–8 days to a desired size of 1.0 cm in diameter (15).

IO-YAS Microparticle Preparation and Phantom Studies

Through an established collaboration with the Mo-Sci Corporation (Mo-Sci, Rolla, MO), MPs were designed and synthesized specifically for applications in thermoradiotherapy and MR imaging. These MPs were composed of Fe_3O_4 nanocrystals dispersed throughout the YAS glass with approximately 50% iron oxide by mass. The final glass MPs were between 20 and 64μm and had a specific gravity of 3.59g/cc.

To investigate the potential of these magnetic yttrium MPs to generate heat in the presence of an applied AMF, sample concentrations of 72.5, 110, and 145mg/ml were prepared in 2ml H_2O. A 2ml H_2O sample served as the control. Each sample was placed in a glass vial within a cylindrical methacrylate vial carrier (Kimble Cruse, Vineland, NJ) with the following dimensions: 6.2cm tall, 3.8cm outer diameter, and 1.4cm inner diameter. The vial carrier was selected to insulate the samples from heat dissipated from the induction coil for specific absorption rate (SAR) estimation during early AMF exposures. SAR values expressed in W/g were calculated by taking the product of the heat capacity of water (4.18J/g°C) and the maximum rate of heating (°C/sec), and normalizing by the ratio of sample mass to magnetically susceptible mass. Five independent experiments were completed for each concentration at coil currents of 470, 340, and 300 Amperes (A).

For the above measurements, each sample was placed in a water-cooled Helmholtz-style coil consisting of two 2-turn windings separated by 2.25 inches, each winding with an inner diameter of 2.5 inches and a length of 1 inch (Figure 1). All samples were positioned in the

center of the lower 2-turn winding and applied coil currents were selected by the operator. Temperature was recorded in 15-second intervals by a fiber optic temperature probe (FTP-LN2, Photon Control, British Columbia, Canada) attached to a PC enabled for data acquisition. Initial temperatures were scaled to 24°C in each phantom study such that ΔT would serve as an indicator of energy transferred to the system.

AMF Protocol and Data Analysis

After baseline MRI for tumor confirmation, each anesthetized rat underwent a mini-laparotomy to expose tumors within the left lateral lobe. Three fiber optic temperature probes recorded intra-tumoral, normal hepatic parenchyma (NHP), and rectal temperatures. The NHP probe was placed in the same lobe as the tumor within 2 cm of the tumor periphery. Probes were secured with cyanoacrylate adhesive. Following probe placement, a neodymium magnet was placed in contact with the tumor for magnetic localization similar to reported techniques for magnetic targeting agents in hepatocellular carcinoma (HCC) (16). A syringe containing 250mg of MPs in 0.9% saline solution was used for direct intratumoral injection via a 16G needle to facilitate passage of MPs in small fluid volumes and to minimize residual MPs within the syringe. The neodymium magnet was removed after 30 seconds and the laparatomy was closed in one layer. The incision was wrapped in gauze and each rat was placed supine in a water-cooled Helmholtz-style coil (Figure 2). Baseline temperatures were recorded for one minute after which time the AMF was applied for 24 minutes. Temperatures were recorded for five additional minutes after removal of the AMF.

The AMF was produced by a 2.4kW RF generator (EASYHEAT 2.4, Ameritherm, Scottsville, NY) with controlled coil currents alternating at frequencies of 193–197kHz. For this study, the maximum coil current (470A) would produce estimated field strengths on the order of 16.5kA/m given the coil dimensions and applied frequencies. Assuming a maximal exposed tissue diameter of 2.5 inches (the inner diameter of the coil), non-specific heating due to eddy current contributions would be expected for field strengths greater than 54.1kA/m at the given frequencies of 200kHz and below (17,18).

It was not feasible to maintain constant positioning of the tumor within the coil due to variability in anatomy and the specific site of tumor induction. Therefore, positioning was iteratively optimized intra-procedurally during the first two minutes of AMF exposure (optimal positioning was defined by maximum observed heating rate). Position changes were limited to this two-minute period. The heating rate (°C/min) was defined as the change in temperature over the first 2.5 minutes of AMF exposure. Therapeutic hyperthermia was defined as core tumor temperatures ≥43°C at any point during the 24-minute application of the AMF.

MR Imaging Protocols

All MRI studies were performed using a 3T Magnetom Trio clinical scanner (Siemens Medical Solutions) with custom-built rodent receiver coil (Chenguang Med. Tech. Co.). Along both coronal and transverse orientations, T2-weighted (T2w) turbo spin echo (TSE) scans were performed with a multi-slice acquisition providing complete coverage of the entire liver. T2w TSE MRI parameters were TR/TE = 4500/61ms; slice thickness = 3mm; FOV = 150×150mm^2. On T2w images, long- and short-axis tumor measurements in the transverse view were recorded. Post-injection scans were used to verify MP delivery following AMF exposure. A circular region of interest (ROI) was drawn to measure mean tumor signal intensity before and after MP injection with side-by-side comparison of transverse T2w TSE images.

Histopathology and ICP-OES

Within 1–2 hours after completion of MR imaging, all animals were euthanized and each liver was then explanted. Specimens were embedded in a cryomold with O.C.T. compound (Sakura Finetek, Torrance, CA) and stored at −80°C. Samples were stained with hematoxylin and eosin and sectioned en face with a slice thickness of 50μm to accommodate the large size of the MPs. Tissue slides were digitized at 20X magnification with TissueGnostics' TissueFAXS system (TissueGnostics, Los Angeles, CA).

Sections of tumor and NHP (to assess MP migration or unintended NHP puncture/delivery) taken from the treated lobe were used for ICP-OES measurements. Tissue samples were immediately weighed and stored at −80°C in metal-free 15ml tubes. All samples (~1g) were digested in 6 ml pure grade HNO_3 and diluted with 18 Meg H_2O based on estimated Fe content. Samples were digested at 200°C in a PerkinElmer (Anton Paar) Multiwave 3000 microwave digester. This system was outfitted with a high-pressure rotor for digestion at 70 bar. Samples were analyzed on a PerkinElmer Optima 2000DV ICP-OES spectrometer in radial mode. Matrix matching was used with a blank and three standards.

Statistical Analysis

All data were analyzed with the statistical package STATA (12.1; StataCorp, College Station, Texas). Statistical analyses included t-tests and difference-in-difference regression. Differences were considered statistically significant at *P*-values less than 0.5.

RESULTS

Maximal temperatures within MP sample vials exposed to AMF were proportional to particle concentration and field strength (Figure 3, 30-sec intervals shown for illustration purposes). Overall, power deposition at 470A was similar for samples with different MP concentrations. Liver tumor growth was successful in 21/21 animals on necropsy, with a mean maximum tumor diameter of 1.01 ± 0.18 cm (*n = 14)*, as measured on axial T2-weighted MR images. There were no complications during IO-YAS MP injections or temperature probe implantations and all animals survived the AMF exposure procedure (14/14). On necropsy, no burns, charring, or vaporization of tissues were observed (0/14). Tumor tissues within all (7/7) animals that received a MP injection achieved the 43°C requirement for therapeutic hyperthermia during AMF exposure (Figure 4). No (0/7) animals in the AMF exposure-only group achieved therapeutic hyperthermia within the tumor tissues and none (0/7) these animals demonstrated tumor, NHP, or rectal temperatures increases greater than 39°C. Temperature differences, final resulting temperatures, and heating rates recorded for the tumor, NHP, and rectal probes are shown in Table 1. Within the treated group, the NHP and rectal temperatures were 37.4 ± 0.9 and 36.5 ± 1.0 °C (*P* = 0.0809) at the conclusion of AMF exposure, respectively. For the MP injection group, the change in temperature during AMF exposure for the tumor was significantly higher than that of the NHP (*P* < 0.001).

After MP injection, there was a strong loss of signal at the site of the tumor within post-injection T2w images and artifacts associated with ferromagnetic content of the YAS MPs were present in 7/7 animals. T2w tumor signal intensity within pre-injection images was 1256 ± 344 arbitrary units (a.u., mean ± SD; *n = 7*) versus a post-injection signal intensity of 130 ± 51 a.u. (*n = 7*) following administration of the IO-YAS MPs (Figure 4). The most common artifact (6/7) was bright pile-up at the margin of signal void that extended beyond the tumor boundary in each animal (6/6).

On histopathologic analysis, IO-YAS particles were identified as black MPs within hematoxylin and eosin-stained specimens. The IO-YAS particles were detected within the tumors in (7/7) animals post-injection. Qualitatively, these IO-YAS particles were observed to be heterogeneously clustered within treated tumors; a sparse distribution was also observed within surrounding NHP (Figure 4). Quantitative analysis with ICP-OES confirmed higher Fe concentrations within tumor tissues in the MP injection group with Fe measurements of 15,716.9 ± 13,140.1 ppm and 303.1 ± 245.2 ppm in the tumor and NHP, respectively (Figure 5). The calibration lines were linear over the expected theoretical range of concentrations. The mean tumor:NHP ratio attributable to IO-YAS MPs was 108:1 after subtracting baseline tumor and NHP Fe concentrations.

DISCUSSION

Hyperthermia can increase radiosensitivity and thus may serve as a valuable adjuvant for yttrium-90 radioembolization therapy. During the current pre-clinical study, therapeutic hyperthermia was localized to the site of liver tumors using magnetically functionalized IO-YAS MPs and external application of an AMF. These IO-YAS MPs were readily visualized under MRI and quantitative ICP-OES confirmed selective intra-tumoral delivery. MPs and/or microspheres fabricated using magnetically functionalized IO-YAS materials should enable the development of concurrent loco-regional thermoradiotherapy for the treatment of liver tumors.

Yttrium content by mass for these IO-YAS MPs was roughly 15.8% versus 45.8% in the glass yttrium-90 microspheres currently approved for the treatment of HCC (TheraSpheres; MDS Nordion, Ottawa, ON, Canada). The optimal activity level for individual microspheres (dependent upon both yttrium content and time between activation and infusion) remains unclear and there are two clinically available options providing lower activities per microsphere than conventional glass microspheres: Extended-shelf-life glass ^{90}Y microspheres and resin ^{90}Y microspheres (SIR-Spheres; Sirtex Medical, Lane Cove, Australia) (19,20). Similar to IO-YAS MPs, the glass yttrium-90 microspheres used clinically (TheraSpheres) are typically 20–40μm in diameter with specific gravities of 3.2–3.6g/cc (19,21).

RF energy alone and coil proximity (AMF exposure group) resulted in mild temperature increases without eddy current burning or vaporization of subcutaneous tissues. While tumors achieved therapeutic temperatures *in vivo* within 4 min 15 seconds of treatment on average, ideal SARs usually exceed 30W/g. The SARs reported are only applicable for the specific field strengths, frequencies, and particle/tissue properties studied. Heterogeneous clusters were evident on pathology and irregularities of tissue thermal conductivities, complex anatomical geometries, and dynamic blood flow effects also complicate delivered thermal distributions. Heat-sink effects due to perfusion can reduce tumor temperatures during hyperthermia procedures (22) and additional work to improve the efficiency and homogeneity of power deposition to the tumor may be needed in the setting of larger animals and/or increased perfusion prior to clinical translation.

Hypoxic cells that are often resistant to radiation can serve as a nidus for local recurrence after radiotherapy but these cells also tend to be considerably more sensitive to hyperthermia than normoxic cells (3–5). Transcatheter embolization acutely increases tumor hypoxia (23) and responses to hypoxia portend worsened survival in human patients after transcatheter arterial chemoembolization (24). The influence of acute and chronic tumor hypoxia on efficacy following sub-stasis ^{90}Y radioembolization where permanently implanted doses are completely absorbed over time should be a challenging and rewarding topic of future investigation.

Reports of yttrium-90 radioembolization as a bridge to resection, RF ablation or transplantation in select patients (25,26) highlight an emerging role for radioembolization in downstaging patients suggesting potential for improved survival. Radioembolization has also become an influential treatment alternative for patients with portal vein thrombosis but diminished liver function at the time of tumor progression often results in ineligibility for systemic therapy in a majority of patients (27). Provided the long history of hyperthermia in radiation therapies, co-localized hyperthermia as a loco-regional adjuvant to radioembolization may improve rates of local control and/or downstaging while preserving liver function in select patients. Future studies are critically necessary to investigate hyperthermia in this setting, to address technical challenges for heating deep-seated tumors, and to advance knowledge of thermal dosimetry effects.

IO-YAS MPs were readily visible on MRI producing image artifacts including focal signal losses due to large dephasing regions and adjacent regions of bright signal bands due to signal pile-up. These findings are consistent with those observed in metallic implants (28) and result from the relatively high Fe_3O_4 content of these IO-YAS MPs. Thus, conventional T2-weighted MRI methods can be used for rapid qualitative depiction of intra-hepatic distributions. The implementation of ultra-short echo-time methods to overcome static dephasing artifacts by sampling T2* decay before the signal reaches the noise floor (29) or gradient echo sampling of the spin echo to sample the rephasing and dephasing components of the spin echo (30) could be valuable to permit quantitative MRI measurements of IO-YAS MP distributions. Reduced T2* in the presence of IO may preclude measurement of proton resonance frequency shifts for MR thermometry (31) and innovative strategies for thermometry are needed at this time.

The present study has several limitations. Direct injection may have allowed increased clustering of MPs in comparison to transcatheter delivery and assessment in larger animal models is necessary. Anesthesia can influence thermoregulation in the rodent model (32) but it was not possible to control for the influences of anesthesia at the levels of perfusion and cellular metabolism. Early or longitudinal responses (on histology or with MRI) were not assessed. Importantly, fibrosis could alter heat transfer and perfusion changes during therapy. Given the absence of fibrosis in our model, this work may be more representative of metastatic hepatic lesions such as those from colorectal carcinoma rather than tumors within the cirrhotic livers often encountered in primary HCC. Signal voids on MRI confirm delivery but may also obscure tumors potentially necessitating alternative imaging techniques such as triphasic computed tomography or positron emission tomography for radiologic response assessments.

The short tissue penetration of yttrium-90 spares the vast majority of normal hepatic parenchyma following radioembolization; this feature may be particularly important in patients with limited hepatic reserve. A new technique for concurrent delivery of intra-tumoral hyperthermia was presented; this loco-regional approach may one day offer to further reduce toxicities to normal hepatic parenchyma given that malignant cells are generally more responsive to hyperthermia-based radiosensitization than normal tissues. With this technology, hyperthermia as a loco-regional adjuvant to yttrium-90 radioembolization is now feasible and further investigation is warranted to evaluate therapeutic efficacy and image-guidance in liver-directed therapy.

Acknowledgments

A special thanks to Jodi Nicolai for cell culture support. The outside support for microparticle digestion and ICP-OES provided by Rudiger Laufhutte of the University of Illinois at Urbana-Champaign was invaluable.

References

1. Valdagni R, Amichetti M. Report of long-term follow-up in a randomized trial comparing radiation therapy and radiation therapy plus hyperthermia to metastatic lymph nodes in stage IV head and neck patients. Int J Radiat Oncol Biol Phys. 1994; 28(1):163–9. [PubMed: 8270437]
2. Sneed PK, Stauffer PR, McDermott MW, et al. Survival benefit of hyperthermia in a prospective randomized trial of brachytherapy boost +/− hyperthermia for glioblastoma multiforme. Int J Radiat Oncol Biol Phys. 1998; 40(2):287–95. [PubMed: 9457811]
3. Overgaard J. Effect of hyperthermia on malignant cells in vivo. A review and a hypothesis. Cancer. 1977; 39(6):2637–46. [PubMed: 872062]
4. Hildebrandt B, Wust P, Ahlers O, et al. The cellular and molecular basis of hyperthermia. Crit Rev Oncol Hematol. 2002; 43(1):33–56. [PubMed: 12098606]
5. Horsman MR, Overgaard J. Hyperthermia: a potent enhancer of radiotherapy. Clin Oncol-Uk. 2007; 19(6):418–26.
6. Gilchrist RK, Medal R, Shorey WD, Hanselman RC, Parrott JC, Taylor CB. Selective inductive heating of lymph nodes. Ann Surg. 1957; 146(4):596–606. [PubMed: 13470751]
7. Maier-Hauff K, Ulrich F, Nestler D, et al. Efficacy and safety of intratumoral thermotherapy using magnetic iron-oxide nanoparticles combined with external beam radiotherapy on patients with recurrent glioblastoma multiforme. J Neuro-Oncol. 2011; 103(2):317–24.
8. Johannsen M, Gneveckow U, Thiesen B, et al. Thermotherapy of prostate cancer using magnetic nanoparticles: feasibility, imaging, and three-dimensional temperature distribution. Eur Urol. 2007; 52(6):1653–61. [PubMed: 17125906]
9. Moroz P, Jones SK, Winter J, Gray BN. Targeting liver tumors with hyperthermia: ferromagnetic embolization in a rabbit liver tumor model. J Surg Oncol. 2001; 78(1):22–9. 30–1. [PubMed: 11519064]
10. Lee K-H, Liapi E, Vossen JA, et al. Distribution of iron oxide-containing Embosphere particles after transcatheter arterial embolization in an animal model of liver cancer: Evaluation with MR Imaging and implication for therapy. J Vasc Interv Radiol. 2008; 19(10):1490–6. [PubMed: 18755602]
11. Kobeiter H, Georgiades CS, Leakakos T, Torbenson M, Hong K, Geschwind J-F. Targeted transarterial therapy of Vx-2 rabbit liver tumor with Yttrium-90 labeled ferromagnetic particles using an external magnetic field. Anticancer Res. 2007; 27(2):755–60. [PubMed: 17465199]
12. Hafeli U, Sweeney S, Beresford B, Humm J, Macklis R. Effective Targeting of Magnetic Radioactive Y-90 Microspheres to Tumor-Cells by an Externally Applied Magnetic-Field - Preliminary In-vitro and In-vivo Results. Nucl Med Biol. 1995; 22(2):147–55. [PubMed: 7767307]
13. Gupta T, Virmani S, Neidt TM, et al. MR tracking of iron-labeled glass radioembolization microspheres during transcatheter delivery to rabbit VX2 liver tumors: feasibility study. Radiology. 2008; 249(3):845–54. [PubMed: 18840788]
14. Adair ER, Black DR. Thermoregulatory responses to RF energy absorption. Bioelectromagnetics. 2003; (Suppl 6):S17–38. [PubMed: 14628305]
15. Guo Y, Zhang Y, Klein R, et al. Irreversible electroporation therapy in the liver: longitudinal efficacy studies in a rat model of hepatocellular carcinoma. Cancer Res. 2010; 70(4):1555–63. [PubMed: 20124486]
16. Wilson M, Kerlan R, Fidelman N, et al. Hepatocellular carcinoma: Regional therapy with a magnetic targeted carrier bound to doxorubicin in a dual MR imaging/conventional angiography suite - Initial experience with four patients. Radiology. 2004; 230(1):287–93. [PubMed: 14695402]
17. Atkinson WJ, Brezovich IA, Chakraborty DP. Usable frequencies in hyperthermia with thermal seeds. IEEE Trans Biomed Eng. 1984; 31(1):70–5. [PubMed: 6724612]
18. Stauffer PR, Cetas TC, Fletcher AM, et al. Observations on the use of ferromagnetic implants for inducing hyperthermia. IEEE Trans Biomed Eng. 1984; 31(1):76–90. [PubMed: 6724613]
19. Kennedy AS, Nutting C, Coldwell D, Gaiser J, Drachenberg C. Pathologic response and microdosimetry of (90)Y microspheres in man: review of four explanted whole livers. Int J Radiat Oncol Biol Phys. 2004; 60(5):1552–63. [PubMed: 15590187]

20. Lewandowski RJ, Riaz A, Ryu RK, et al. Optimization of radioembolic effect with extended-shelf-life yttrium-90 microspheres: results from a pilot study. J Vasc Interv Radiol. 2009; 20(12):1557–63. [PubMed: 19854068]
21. Kennedy A, Nag S, Salem R, et al. Recommendations for radioembolization of hepatic malignancies using yttrium-90 microsphere brachytherapy: a consensus panel report from the radioembolization brachytherapy oncology consortium. Int J Radiat Oncol Biol Phys. 2007; 68(1): 13–23. [PubMed: 17448867]
22. Wilkins LR, Wu H, Haaga JR, Exner A. Radiofrequency ablation: effect of tumor- and organ-specific pharmacologic modulation of arterial and portal venous blood flow on coagulation diameter in an N1-S1 tumor model. J Vasc Interv Radiol. 2012; 23(6):826–32. [PubMed: 22507596]
23. Virmani S, Rhee TK, Ryu RK, et al. Comparison of hypoxia-inducible factor-1alpha expression before and after transcatheter arterial embolization in rabbit VX2 liver tumors. J Vasc Interv Radiol. 2008; 19(10):1483–9. [PubMed: 18922400]
24. Sergio A, Cristofori C, Cardin R, et al. Transcatheter arterial chemoembolization (TACE) in hepatocellular carcinoma (HCC): the role of angiogenesis and invasiveness. Am J Gastroenterol. 2008; 103(4):914–21. [PubMed: 18177453]
25. Kulik LM, Atassi B, van Holsbeeck L, et al. Yttrium-90 microspheres (TheraSphere) treatment of unresectable hepatocellular carcinoma: downstaging to resection, RFA and bridge to transplantation. J Surg Oncol. 2006; 94(7):572–86. [PubMed: 17048240]
26. Lewandowski RJ, Kulik LM, Riaz A, et al. A comparative analysis of transarterial downstaging for hepatocellular carcinoma: chemoembolization versus radioembolization. Am J Transplant. 2009; 9(8):1920–8. [PubMed: 19552767]
27. Memon K, Kulik L, Lewandowski RJ, et al. Radioembolization for hepatocellular carcinoma with portal vein thrombosis: impact of liver function on systemic treatment options at disease progression. J Hepatol. 2013; 58(1):73–80. [PubMed: 23000237]
28. Hargreaves BA, Worters PW, Pauly KB. Metal-Induced Artifacts in MRI. Am J of Roentgenology. 2011; 197(3):547–555.
29. Robson MD, Gatehouse PD, Bydder M, Bydder GM. Magnetic resonance: an introduction to ultrashort TE (UTE) imaging. J Comput Assist Tomogr. 2003; 27(6):825–46. [PubMed: 14600447]
30. Yablonskiy DA, Haacke EM. An MRI method for measuring T2 in the presence of static and RF magnetic field inhomogeneities. Magn Reson Med. 1997; 37(6):872–6. [PubMed: 9178238]
31. Wlodarczyk W, Hentschel M, Wust P, et al. Comparison of four magnetic resonance methods for mapping small temperature changes. Phys Med Biol. 1999; 44(2):607–24. [PubMed: 10070804]
32. Davis JA. Mouse and rat anesthesia and analgesia. Curr Protoc Neurosci. 2008 Appendix4B.

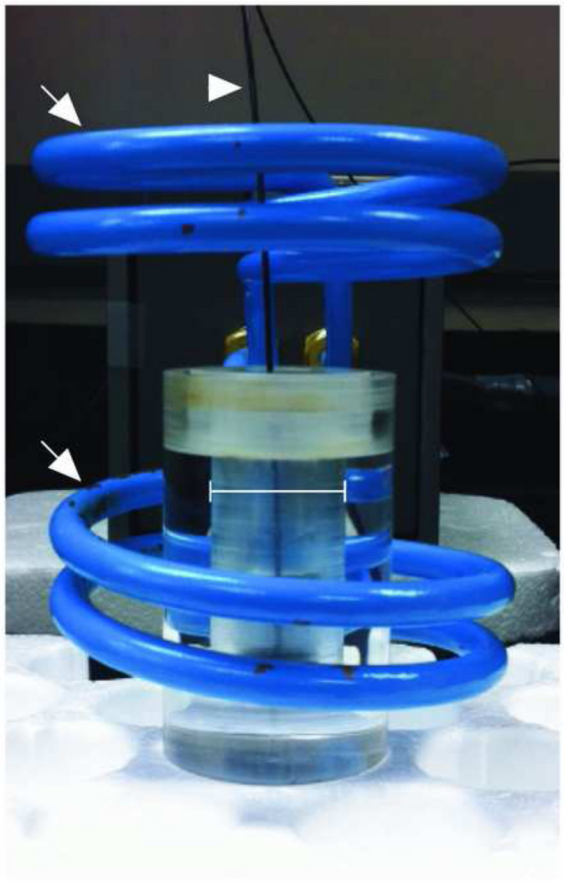

Figure 1.
Positioning of methacrylate vial carrier (bar denotes vial within carrier), sample, and temperature probe (arrowhead) within the induction coil (arrows).

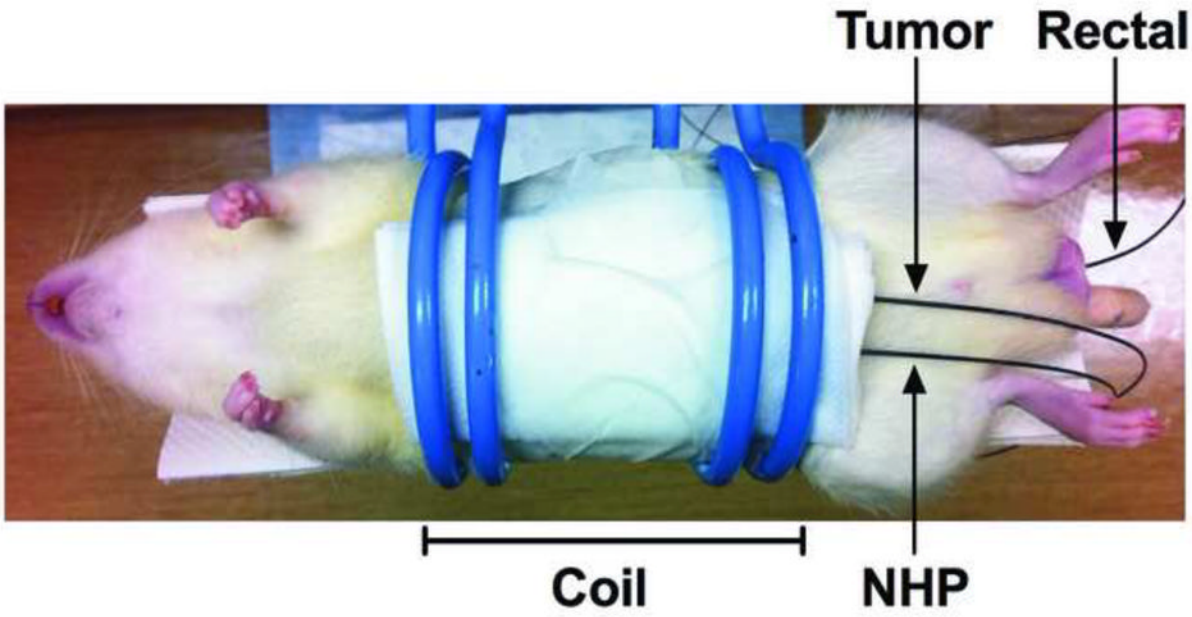

Figure 2.
Initial coil position (bar) during *in vivo* application of AMF. Three fiber optic temperature probes permitted simultaneous measurement of tumor, NHP, and rectal temperatures.

Figure 3a

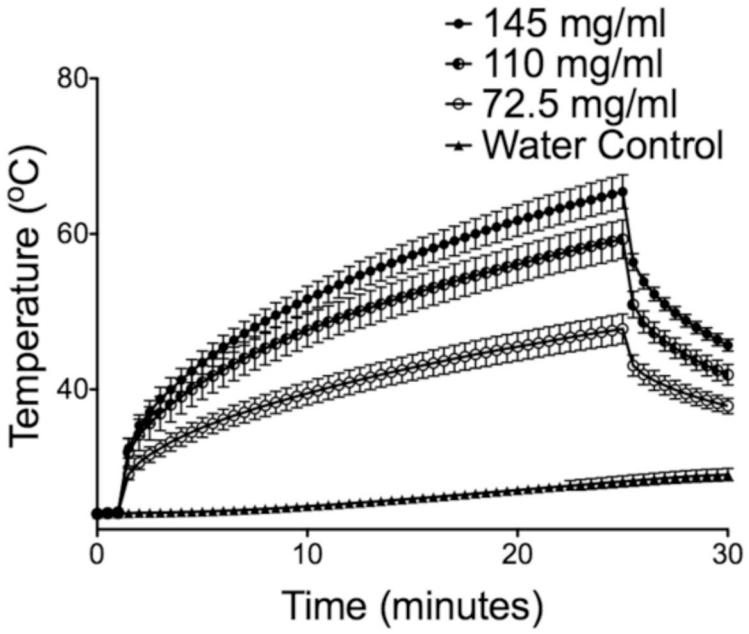

Figure 3b

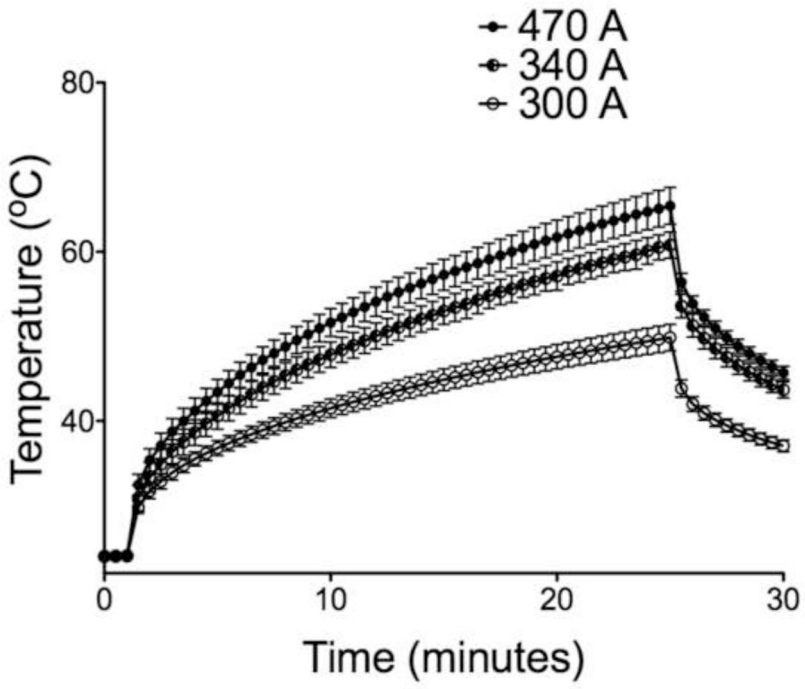

Figure 3.

(a) SARs for 470A coil current at 193kHz were 23.3, 28.7, and 26.8 W/g for 145, 110, and 72.5 mg/ml respectively (*n=5*). (b) For a concentration of 145mg/ml, coil currents of 470, 340, 300A at 193kHz produced SARs of 23.3, 17.58, and 15.56 W/g (*n=5*). Bars indicate standard deviation.

Figure 4a

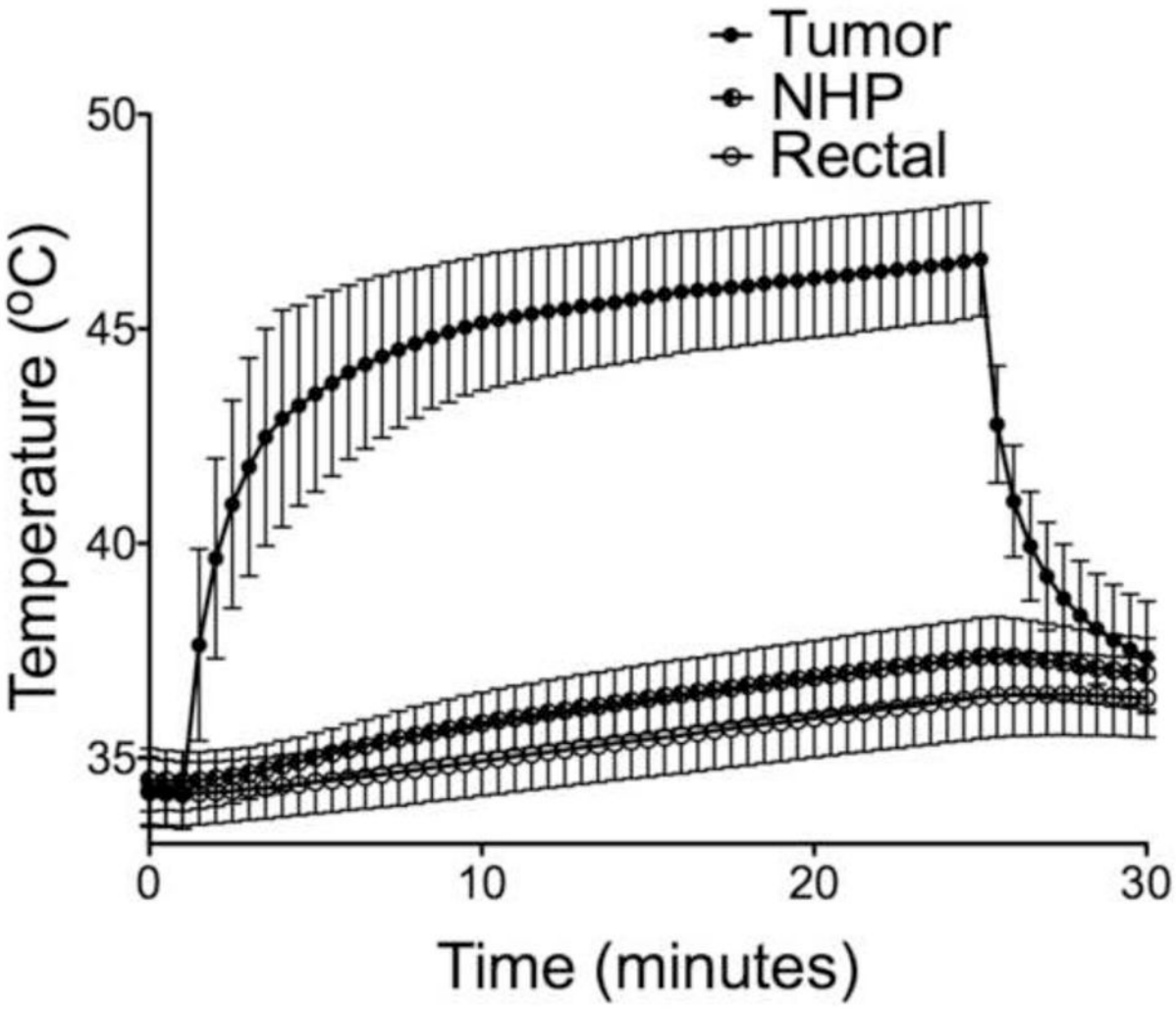

Figure 4b

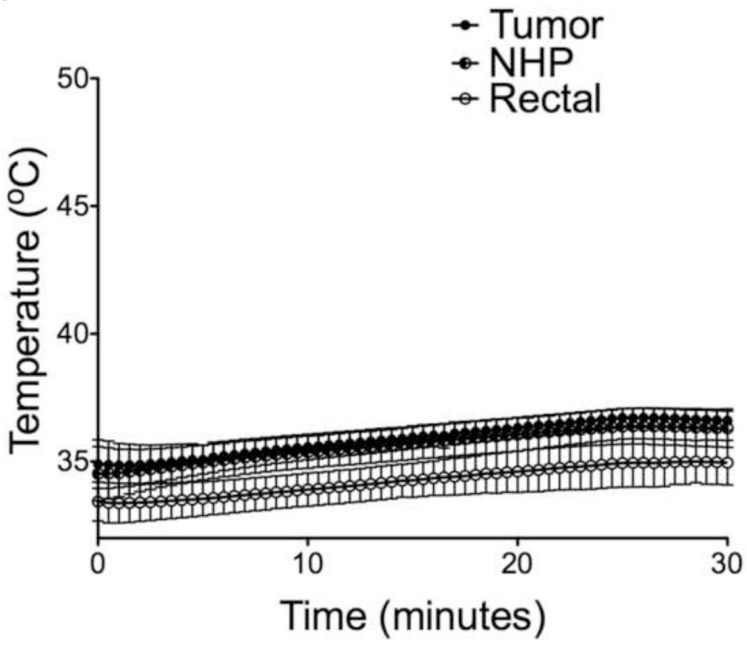

Figure 4.

(a) Temperature measurements in the tumor, NHP, and rectum following intra-tumoral MP injection (*n=7*). (b) Temperature measurements in the control tumor, NHP, and rectum (*n=7*). Bars indicate standard deviation.

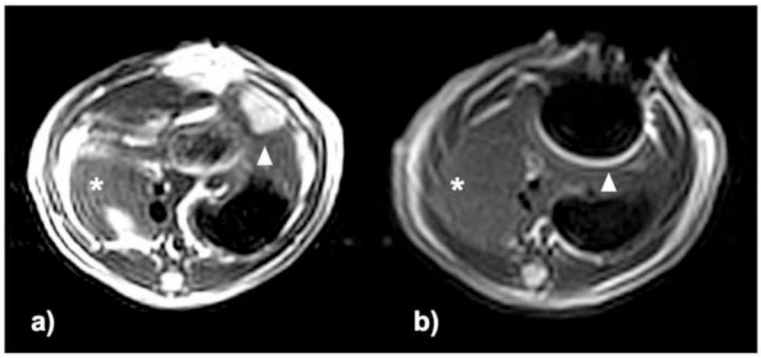

Figure 5.
T2w TSE images (axial view) (a) pre- and (b) post-injection. Within T2w images, left lateral lobe tumors were hyperintense relative to adjacent NHP (arrowhead indicates tumor position) and normal median lobe (asterisk). Post-injection images show signal voids corresponding to the location of the tumor and bright pile-up artifacts (arrowhead) in the phase-encoding direction that were not present in the normal median lobe (asterisk).

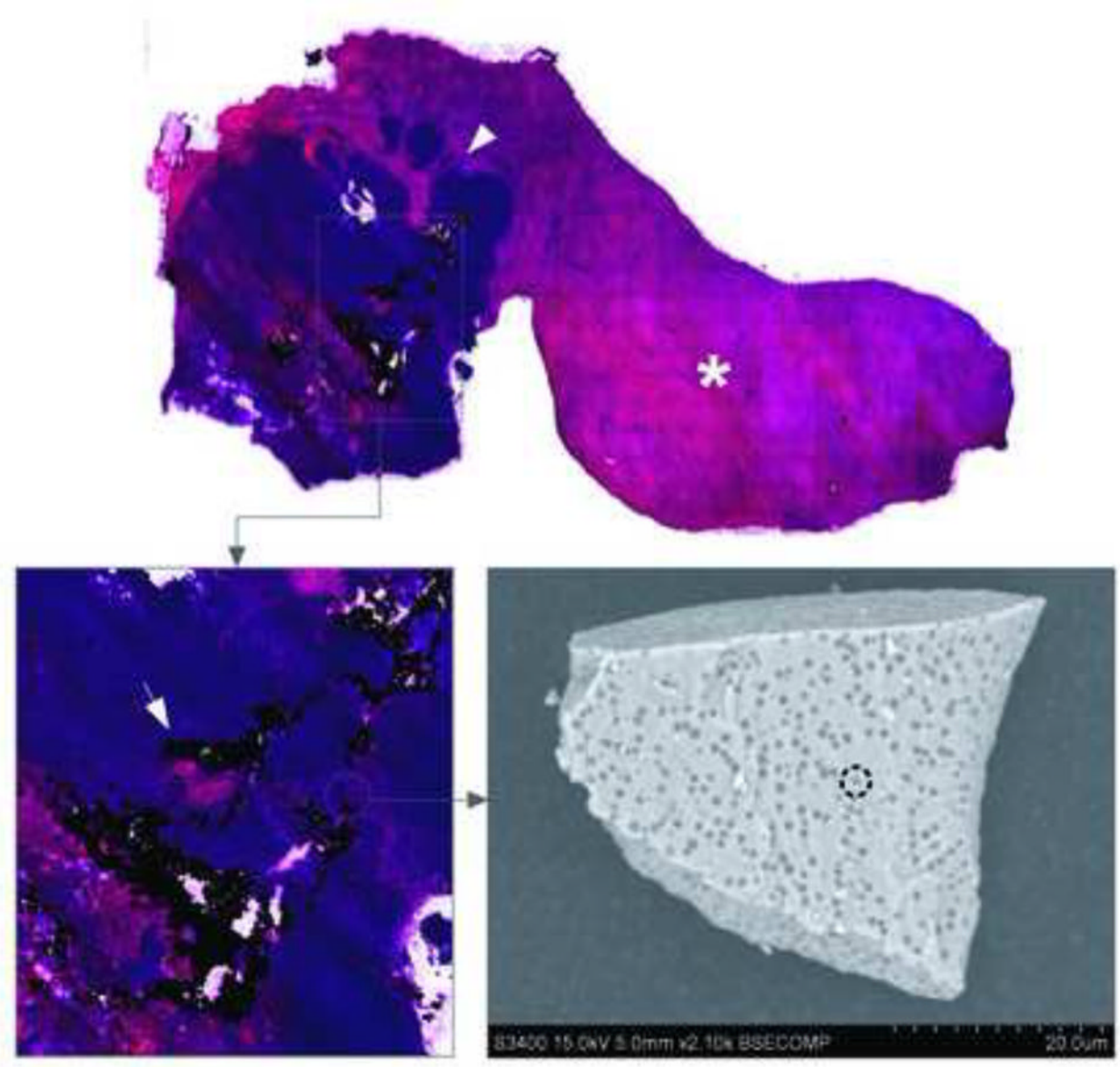

Figure 6.

Hematoxylin and eosin-stained liver lobe following IO-YAS MP injection. Dense intra-tumoral IO-YAS MP clusters (arrow) were observed within the tumor (arrowhead) with few particles in the NHP (asterisk). SEM of a single IO-YAS MP shows electron dense iron oxide (interrupted circle) embedded within the glass yttrium aluminosilicate matrix.

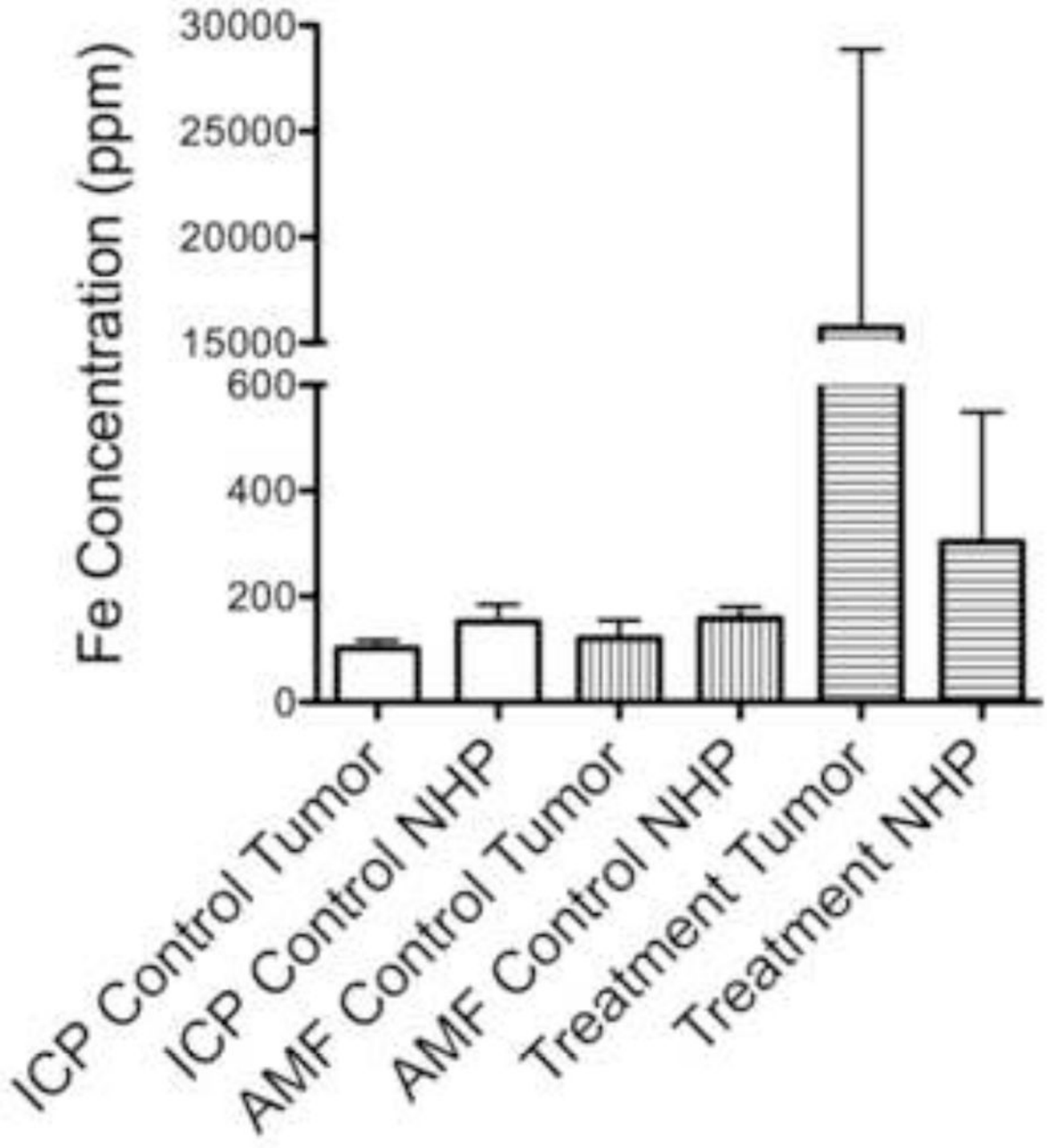

Figure 7.
Localized intra-tumoral delivery. Isolated AMF (without MP injection) and procedural exposure did not significantly influence tumor or NHP [Fe] nor tumor:NHP ratios as measured by ICP-OES. Direct injection of IO-YAS MPs with magnetic targeting under direct vision yielded a mean tumor:NHP Fe ratio of 75.2 versus 0.77 in the AMF control group ($P < 0.05$).

TABLE 1

AMF Temperature Probe Measurements *in vivo*

	Group	Tumor	NHP	Rectal
	HT	12.50 ± 1.56	2.9 ± 1.08	2.25 ± 0.79
ΔT (°C)	C_{AMF}	1.86 ± 0.75	1.68 ± 0.97	1.57 ± 1.17
	P Value:	0.0156	0.0469	0.4688
	HT	46.62 ± 1.43	37.40 ± 0.98	36.53 ± 1.07
T_{final} *(°C)*	C_{AMF}	36.76 ± 0.39	36.44 ± 0.75	35.06 ± 0.93
	P Value:	< 0.0001	0.1279	0.0182
	HT	3.34 ± 1.06	0.11 ± 0.11	0.05 ± 0.06
Rate (°C/min)	C_{AMF}	0.05 ± 0.10	0.10 ± 0.10	0.04 ± 0.09
	P Value:	< 0.0001	0.9059	0.7132

Note.–Values expressed as means ± SD where applicable.

AMF = alternating magnetic field, C = control, HT = hyperthermia, NHP = normal hepatic parenchyma, ΔT = temperature change, T_{final} = post-treatment temperature.